








RESEARCH ARTICLE | MARCH 03 2025

Polarization rotation in a ferroelectric BaTiO₃ film through low-energy He-implantation

Andreas Herklotz ; Robert Roth; Zhi Xiang Chong ; Liang Luo ; Joong Mok Park ; Matthew Brahlek ; Jigang Wang ; Kathrin Dörr; Thomas Zac Ward 



APL Mater. 13, 031105 (2025)

<https://doi.org/10.1063/5.0253298>



View
Online



Export
Citation

Articles You May Be Interested In

Effect of fabrication processes on BaTiO₃ capacitor properties

APL Mater. (April 2024)

BaTiO₃/SrTiO₃ heterostructures for ferroelectric field effect transistors

Appl. Phys. Lett. (June 2017)

Ferroelectric and ferromagnetic properties in BaTiO₃ thin films on Si (100)

J. Appl. Phys. (September 2014)

APL Materials

Now Online: Roadmap articles

[Read Now](#)

Polarization rotation in a ferroelectric BaTiO₃ film through low-energy He-implantation

Cite as: APL Mater. 13, 031105 (2025); doi: 10.1063/5.0253298

Submitted: 16 December 2024 • Accepted: 10 February 2025 •

Published Online: 3 March 2025



Andreas Herklotz,^{1,a)} Robert Roth,^{1,b)} Zhi Xiang Chong,² Liang Luo,^{2,3} Joong Mok Park,^{2,3} Matthew Brahelek,⁴ Jigang Wang,^{2,3} Kathrin Dörr,¹ and Thomas Zac Ward⁵

AFFILIATIONS

¹ Institute for Physics, Martin-Luther-University Halle-Wittenberg, Halle, Germany

² Department of Physics and Astronomy, Iowa State University, Ames, Iowa 50011, USA

³ Ames National Laboratory, Ames, Iowa 50011, USA

⁴ Materials Science and Technology Division, Oak Ridge National Laboratory, Oak Ridge, Tennessee 37830, USA

⁵ Center for Nanophase Materials Sciences, Oak Ridge National Laboratory, Oak Ridge, Tennessee 37830, USA

^{a)} Author to whom correspondence should be addressed: herklotza@gmail.com

^{b)} Deceased.

ABSTRACT

Domain engineering in ferroelectric thin films is crucial for next-generation microelectronic and photonic technologies. Here, a method is demonstrated to precisely control domain configurations in BaTiO₃ thin films through low-energy He ion implantation. The approach transforms a mixed ferroelectric domain state with significant in-plane polarization into a uniform out-of-plane tetragonal phase by selectively modifying the strain state in the film's top region. This structural transition significantly improves domain homogeneity and reduces polarization imprint, leading to symmetric ferroelectric switching characteristics. The demonstrated ability to manipulate ferroelectric domains post-growth enables tailored functional properties without compromising the coherently strained bottom interface. The method's compatibility with semiconductor processing and ability to selectively modify specific regions make it particularly promising for practical implementation in integrated devices. This work establishes a versatile approach for strain-mediated domain engineering that could be extended to a wide range of ferroelectric systems, providing new opportunities for memory, sensing, and photonic applications where precise control of polarization states is essential.

© 2025 Author(s). All article content, except where otherwise noted, is licensed under a Creative Commons Attribution-NonCommercial-NoDerivs 4.0 International (CC BY-NC-ND) license (<https://creativecommons.org/licenses/by-nc-nd/4.0/>). <https://doi.org/10.1063/5.0253298>

INTRODUCTION

Controlling domain configurations in ferroelectric thin films is one of the most crucial avenues to unlock functionalities in ferroic heterostructures. For example, domain engineering has been shown to be of vital importance in ferroelectric memristors, domain-wall memories, and nanocircuitry.¹ New ferroelectric nanoelectronics often rely on the fine-tuning and manipulation of domain walls² or the creation of complex polar topologies,³ both requiring the control of depolarization fields and lattice anisotropy.

Highly efficient domain engineering thus requires a material system with a high sensitivity toward competing polar and structural phases. A prototype ferroelectric with a multitude of potential

domain states is perovskite BaTiO₃ (BTO). Bulk BTO is a rhombohedral ferroelectric in its ground state and crosses a series of orthorhombic and tetragonal phases until it reaches cubic symmetry above the Curie temperature of about 110 °C.⁴ The extraordinary properties of BTO have made it a cornerstone material for numerous technological applications, from high-density capacitors to piezoelectric actuators. Recently, BTO's strong Pockels effect⁵ has drawn significant interest for next-generation electro-optic devices in quantum photonic integrated circuits.⁶ While conventional approaches using BTO have demonstrated impressive modulation capabilities for classical optical signals,⁷ emerging quantum information applications demand precise control over domain configurations to maximize electro-optic coefficients while

minimizing optical losses from domain walls and structural inhomogeneities.⁸ The ability to deterministically engineer BTO's ferroelectric domain structure could enable high-speed modulators operating at GHz frequencies, essential for quantum information processing, while maintaining compatibility with existing semiconductor fabrication processes. However, achieving such control remains challenging using traditional strain engineering approaches, which are limited by available substrate materials and critical thickness constraints.

An efficient way to engineer domain structures in BTO thin films has been epitaxial strain. Early work has shown that biaxial in-plane strain of only about one percent can shift the ferroelectric transition temperature upward by several hundred Kelvin.⁹ Similarly, domain configurations are effectively altered under biaxial strain. A complex balance of mostly in-plane oriented monoclinic domains in the form of a regular zigzag lamella pattern was observed for a low-strain film grown on NdScO₃ substrates,¹⁰ while larger compressive strain as grown on DyScO₃ or GdScO₃ substrates leads to stabilization of the tetragonal phase with predominantly out-of-plane oriented domains.¹¹ These experimental observations have been in good agreement with phase field simulations based on phenomenological Landau–Ginzburg–Devonshire theory.^{12,13}

A drawback of epitaxial strain is the need for suitable single crystal substrates to achieve desired strain states. In addition, strain relaxation occurs above a critical film thickness, which may permit the stabilization of the targeted strain. Alternative approaches to induce lattice strain in a continuous and controllable way may allow access to new domain configurations that are otherwise impossible to achieve by standard strain engineering. In our previous work, we have introduced the strain doping approach, where low-energy He ion implantation is used to create a unit cell expansion in thin films.^{14,15} This expansion may be caused by the ion incorporation into the lattice itself, or through a secondary effect, such as the creation of oxygen vacancies. In epitaxial thin films, the volume expansion is typically equivalent to a uniaxial out-of-plane expansion, since the in-plane lattice remains epitaxially locked to the substrate. The out-of-plane strain can then be continuously controllable via the ion implantation dose and has been used to manipulate magnetic,^{16,17} dielectric,^{18,19} and transport properties²⁰ across a range of oxide films.

In this work, we apply strain doping to epitaxial BTO films. We show that the uniaxial strain induced by ion implantation induces a phase transition from a mixed domain to a purely out-of-plane oriented tetragonal domain state. This transition is tantamount to a ferroelectric polarization rotation from in-plane to out-of-plane. We argue that, due to the universal character of strain doping, polarization rotation can also successfully be induced in a wide range of other ferroelectric or ferroelastic systems.

RESULTS

A BTO (80 nm)/LSMO (10 nm) film is deposited on a (110) DyScO₃ substrate, capped with 15 nm thick Au electrodes and subsequently implanted with 5 keV He ions. No surface modification could be seen compared to the as-grown film after the mechanical removal of the protective Au layer. A schematic illustration of

the heterostructure is presented in Fig. 1(a). The dimensionless He implantation profile, as estimated by a Monte Carlo simulation, is included as a bar graph. The majority of the He ions are expected to stop within the first half of the BTO layer. Figure 1(b) shows a x-ray diffraction (XRD) reciprocal space map around the (103)_{pc} reflections of the as-grown heterostructure. While the LSMO layer is coherently strained to the substrate, the BTO film shows some degree of strain-relaxation. The pseudocubic lattice parameter of the scandate ($a_{\text{DSO}} = 3.944 \text{ \AA}$) provides a compressive lattice mismatch of -1.2% to the a -parameter of the tetragonal titanate bulk lattice structure ($a_{\text{BTO}} = 3.992 \text{ \AA}$, $c_{\text{BTO}} = 4.036 \text{ \AA}$).^{21–23} Previous work has revealed that epitaxial BTO films tend to release misfit strain throughout the film growth, leaving a bottom strained part and a strain-relaxed top part.²⁴ This behavior is reflected in our XRD measurements. The zoomed-in reciprocal space map clearly reveals the presence of a coherently strained film part, represented by a single peak, and a fully relaxed film part, represented by an agglomeration of three sub-peaks. From the intensity ratio of the two BTO peaks, we estimate that the strained part is 20–35 nm thick. Having a single uniform peak indicates that the bottom film part has a tetragonal structure with $a = 3.944 \text{ \AA}$ and $c = 4.069 \text{ \AA}$ and is made up of c -oriented ferroelectric domains. This tetragonal strained state will be called the T-phase. The peak splitting of the top part is a consequence of a symmetry change under strain-relaxation. A splitting into three peaks within the H0L plane can be explained by the presence of M_C-type monoclinic domains with polarization vectors within the (100)_{pc} and (010)_{pc} plane. A detailed structural clarification is difficult, since different domain configurations, such as mixed rhombohedral/orthorhombic configurations, can lead to the same XRD peak pattern. Throughout the remainder of the text, we will refer to this strain-relaxed domain state as the R-phase, referring to the rhombohedral strain-free bulk-like state. It should be noted that the conclusions throughout this paper are not affected by this uncertainty, since in all cases, the crystal symmetry is lower than that of the T-phase and the ferroelectric polarization is rotated away from the film normal.

Figure 1(c) shows the changes in XRD θ – 2θ scans around the pseudocubic 002 reflections with subsequent He ion implantation. A clear double peak behavior associated with the strained and strain-relaxed film part is visible for the as-grown film. Upon ion implantation, the relaxed film peak is shifting to lower 2θ angles to unify with the strained film peak. The natural interpretation of these data is that the top half of the BTO film, which is effectively implanted with He ions, is strained and structurally adapting to the bottom half of the film.

A clearer picture can be derived from the reciprocal space maps of the heterostructure taken at various He implantation levels, shown in Fig. 2. As illustrated schematically on the left, the strained part of the as-grown film has a tetragonal structure with out-of-plane polarization. The strain-relaxed R-phase part has an average polarization that has a significant in-plane polarization component. Under He implantation, the relaxed top part undergoes significant changes. We find that the peak narrows and transforms into a single peak, while the film expands along the c -axes. We interpret this observation as a strain induced structural transition from the R- to T-state. As illustrated on the right of Fig. 2, the lattice of the whole film is elongated along out-of-plane and the polarization is fully aligned along the film normal. He implantation effectively

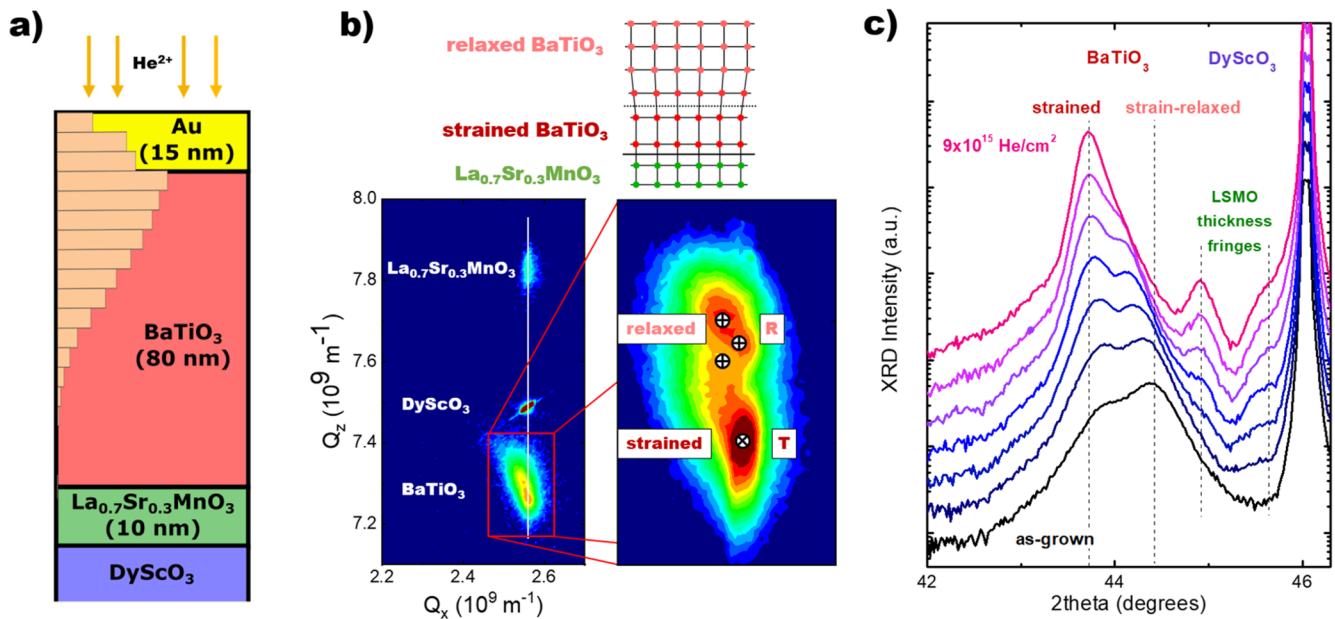


FIG. 1. (a) Schematic representation of the thin film heterostructure studied in this work and the calculated He ion profile. (b) A reciprocal space map around the (103)_{pc} reflection highlights partial strain relaxation throughout the BaTiO₃ film. The zoomed-in image shows the presence of a strained and a relaxed film part. Crosses indicate peak splitting due to structural domain formation. (c) θ -2 θ scans around the (002)_{pc} reflections of the BTO. The scans with varying He implantation levels are shifted vertically for clarity.

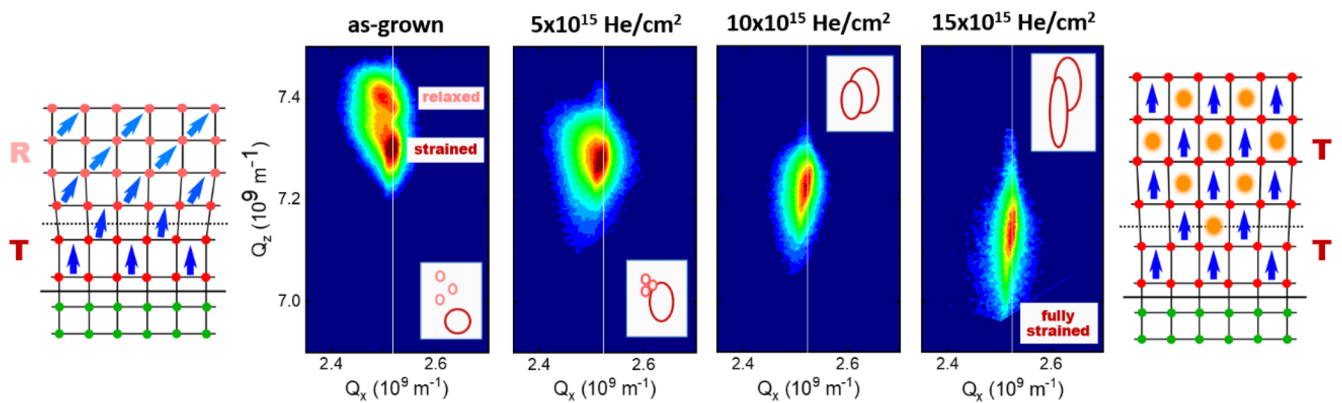


FIG. 2. Series of reciprocal space maps around the (103)_{pc} reflection of the BaTiO₃ film with increasing ion implantation dose. The insets illustrate the positions and shapes of the sub-peaks, with the light red circles reflecting the strain-relaxed top part and the dark red circle reflecting the strained bottom part of the film. The schemes on the left and right illustrate the lattice distortions and Ti off-center displacements (blue arrows) of the as-grown and 15 × 10¹⁵ He/cm² film, respectively.

transforms the inhomogeneous multi-domain film into a structurally more homogeneous purely tetragonal film.

In order to gain additional insights into the symmetry changes induced by He implantation, we have performed second harmonic generation (SHG) measurements on a He implanted BTO heterostructure. Figure 3 shows polar plots of the measured s-polarized (red) and p-polarized (blue) SHG intensity as a function of the polarization angle φ . The measured data are fit to equations that either reflect a purely tetragonal film or a mix of tetragonal and

rhombohedral domains. Detailed information on the experimental setup and derivations of the fitting equations can be found in the [supplementary material](#). When a fully tetragonal crystal structure is assumed for the as-grown film (top left graph), the data cannot be fitted satisfactorily. Small but clear deviations can be seen, highlighted by the blue and red arrows. However, a much better fitting result is achieved if the equations for a tetragonal/rhombohedral phase coexistence are used (bottom left). This result is in agreement with our XRD data, which indicates that the as-grown film is not fully

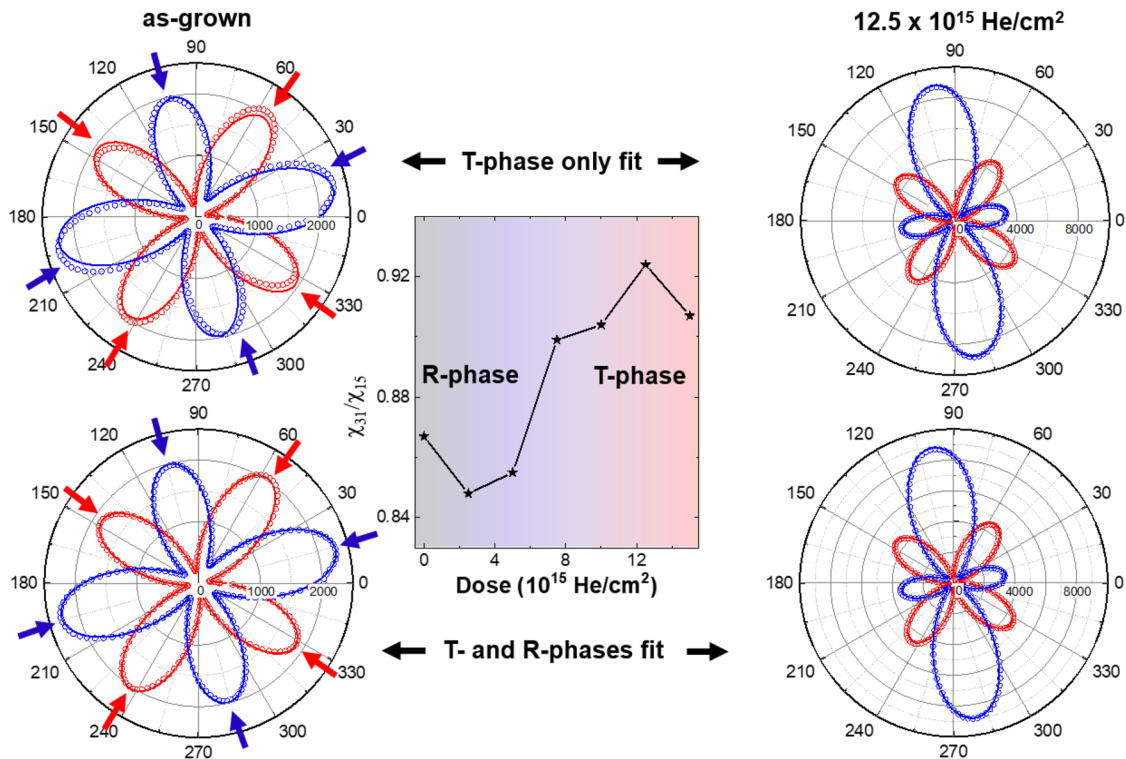


FIG. 3. SHG measurements: Polar plots of the measured s-polarized (red) and p-polarized (blue) SHG intensity as a function of polarization angle φ for the as-grown film and the film implanted with $12.5 \times 10^{15} \text{ He/cm}^2$. Measured data and fits are represented by open symbols and solid lines, respectively. Fits are based on the equations for purely tetragonal phase only (top) and a combination of tetragonal and rhombohedral phases (bottom). The red and blue arrows highlight that the as-grown film requires the addition of a rhombohedral phase content to fit the SHG data satisfactorily. The graph in the middle shows χ_{31}/χ_{15} , as determined from the fitting parameters, as a function of the He dose.

tetragonal and includes parts with lower symmetry. Note that SHG is sensitive to the whole heterostructure, i.e., to the lower tetragonal coherently strained BTO film part as well as the lower symmetry top part. The film implanted with $12.5 \times 10^{15} \text{ He/cm}^2$ shows a significantly different SHG response. This change already indicates that He implantation affects the ferroelectric domain structure of the BTO film. The data can be fitted very well by the equations assuming a purely tetragonal film alone (top right graph). Including the terms for a rhombohedral phase does not improve the fit by a notable degree (bottom right graph). This result suggests that He implantation transforms the mixed phase film into a single-phase tetragonal film.

In the center graph of Fig. 3, we plot the second harmonic generation tensor element ratio χ_{31}/χ_{15} as a function of He dose. The tensor elements, χ_{31}/χ_{15} , are determined by extracting SHG intensity at $\varphi = 90^\circ$ in the p-out feature and $\varphi = 45^\circ$ in the s-out feature. An increase in this ratio toward 1 has been shown to indicate an increase in crystal symmetry.^{25–27} The overall symmetry of the BTO film is increased during He implantation as the film transforms into a purely tetragonal state. Thus, our SHG measurements serve as a powerful tool for unraveling the spatial symmetry evolution of BTO films. Moreover, as the temporal dynamics of lattice symmetry gain increasing significance,^{28,29}

the SHG findings motivate future time-resolved studies employing ultrafast SHG spectroscopy to investigate the temporal behavior of BTO.

In order to corroborate these experimental findings by theory, we have performed phase field simulations based on a Landau–Devonshire thermodynamic potential described more in the Methods section. At first, the domain configuration as a function of in-plane strain is modeled (first row of Fig. 4). Under a large in-plane compressive strain of -1.2% , the film consists entirely of dense $c^{+/-}$ domains. This result is in line with previous theoretical and experimental observations.^{9,12} It is also in agreement with the absence of XRD peak splitting for the fully strained T-phase film part. When a smaller in-plane strain is assumed in our calculations, the density of c domains decreases. For fully strain-free films, a large part of the ferroelectric polarization is tilted away from the film normal through the formation of orthorhombic, rhombohedral, or monoclinic domains. This prediction has been confirmed experimentally in strain-free films before¹⁰ and is reflected in our data by the observation of the R-phase with splitting into multiple XRD peaks.

In a next step, the effect of He implantation on the ferroelectric domain structure was modeled simply by using the strain-free domain configuration as a starting point and sequentially

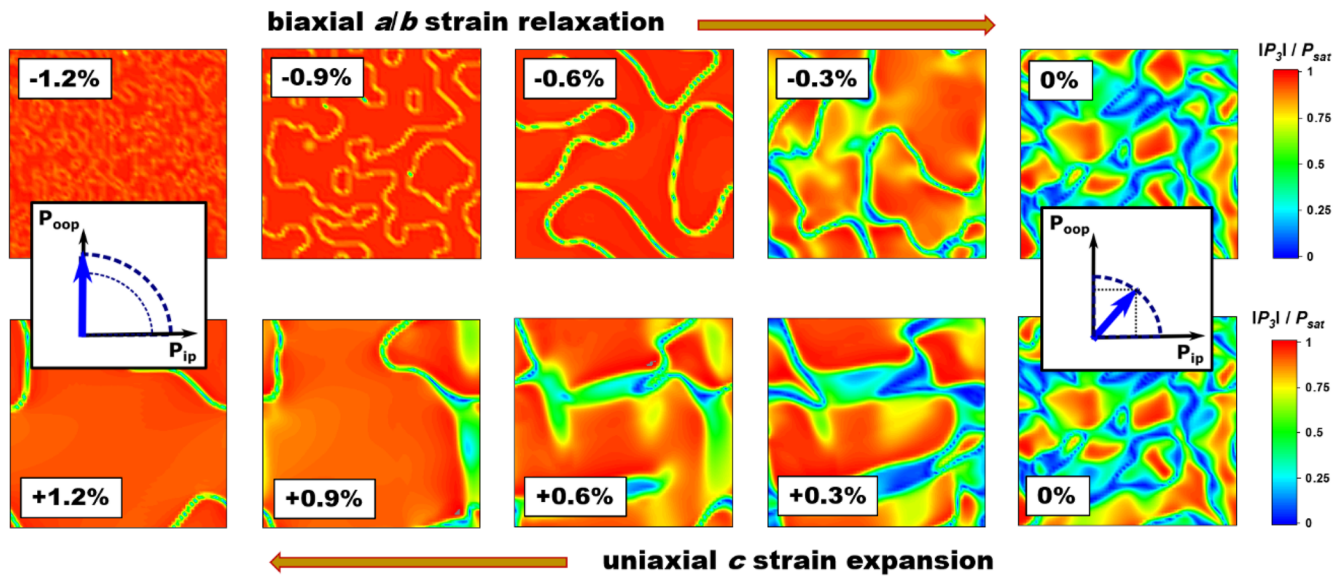


FIG. 4. Out-of-plane polarization component at the top of a BaTiO₃ film as calculated by phase field simulations. The top row highlights the effect of decreasing in-plane strain during strain relaxation, while the bottom row shows the result obtained through the continuous expansion of the out-of-plane axis while the in-plane axis is fixed. The insets schematically illustrate the rotation of the average polarization toward the film normal when biaxial compression and out-of-plane expansion are increased.

expanding the unit cells along the out-of-plane direction. Second order effects, for example through changing material parameters, were neglected. It can be seen that the ferroelectric polarization continuously rotates back into the film normal and a $c^{+/-}$ ferroelectric domain pattern is established. The out-of-plane expansion counteracts in-plane strain-relaxation. This result is consistent with our experimental data, which suggests a strain-induced structural phase transition of the strain-relaxed part toward a fully tetragonal state.

The structural changes upon He implantation have a profound influence on the BTO thin film properties. Macroscopic ferroelectric polarization measurements in capacitor geometry shown in the [supplementary material](#) reveal a remanent out-of-plane polarization of about $27 \mu\text{C}/\text{cm}^2$ for the film with the highest dose. This value is slightly larger than the expected single-crystal value for tetragonal BTO and is, therefore, further evidence for a complete phase transformation under ion implantation. During the

structural transition toward a fully tetragonal film, the uniformity of the film is increased. One might thus expect a reduction in asymmetry in ferroelectric hysteresis loops at lower He doses. In contrast, for higher implantation levels, the strain uniformity is decreasing again since ion implantation is only affecting the strain state in the top part of the film, while the bottom part remains essentially unchanged. This two-region behavior is confirmed in dielectric hysteresis measurements shown in [Fig. 5](#). The hysteresis loop for the as-grown film is slightly asymmetric with a shift to negative voltages. This polarization imprint behavior has been observed repeatedly for epitaxial BaTiO₃ films and has been attributed to asymmetry within the ferroelectric layer,³⁰ as, for example, due to the accumulation of defects near interfaces, and/or the asymmetry induced by the presence of different top and bottom electrodes.⁵ The associated in-built field drives ferroelectric domains to have a favorable orientation, which is downward in our case.³¹

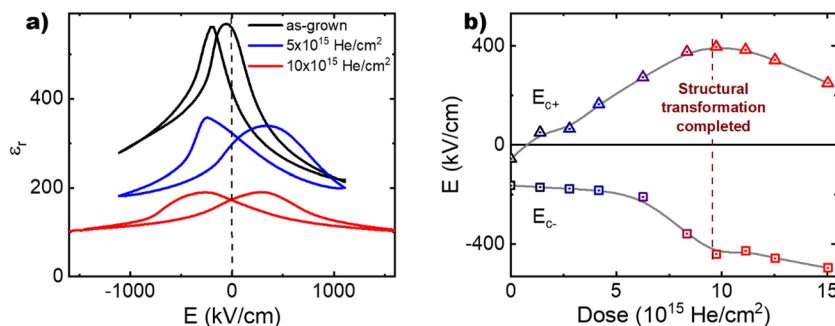


FIG. 5. (a) ϵ - E hysteresis loops for films with different He implantation doses. (b) Coercive fields determined from the hysteresis loops as a function of the He dose.

With He implantation, the hysteresis loops tend to widen, while the dielectric constants are decreasing overall. Both enhanced coercive fields and reduced polarizability are a consequence of the increased defect density introduced due to ion bombardment and have been reported on other material systems before.^{32,33} Part of the decline of the dielectric permittivity may also be attributed to polarization rotation, as the permittivity along the polarization axis is typically smaller than off-axis.³⁴ Interestingly, the coercive fields are increasing at a different rate, as can be seen in Fig. 5(b). At 10×10^{15} He/cm², the hysteresis loop is nearly symmetrical. The polarization imprint is removed. This point coincides with the structurally most uniform state where the structural transformation of the top part is fully completed and the out-of-plane strain state is similar to that of the bottom part. The full film is of T-phase. For higher He doses, the trend in coercive fields is reversed and an overall negative in-built field is created again. In this region, the asymmetry is enhanced again since He ions are only implanted in the top film part, and consequently, the out-of-plane strain further increases past that of the bottom part. The resultant strain gradient is creating a flexoelectric in-built electric field.³⁰

CONCLUSION

Helium ion irradiation is demonstrated to offer precise control over ferroelectric domain orientation in BTO films. This approach is found to enable transformation of an as-grown mixed ferroelectric state, characterized by significant in-plane polarization components in the relaxed top portion of the film, into a uniform out-of-plane tetragonal phase. The structural modification significantly improves domain homogeneity while reducing polarization imprint and restoring symmetric ferroelectric switching characteristics. The ability to selectively modify only the top portion of the film through low-energy ion implantation provides a powerful tool for post-growth domain engineering without affecting the coherently strained bottom interface.

Manipulating domain configurations through *ex situ* ion implantation constitutes an appealing strategy to tailor the switching characteristics of ferroelectric films. We expect that this technology can be applied to a wide range of material systems with different types of ferroelectric and ferroelastic domain patterns. As an example, the ability to precisely control ferroelectric domains in BTO films through He ion implantation has significant implications for quantum photonic integrated circuits, where efficient electro-optic modulation and low propagation losses are critical. The demonstrated transformation to a uniform out-of-plane polarization state could enhance the Pockels effect needed for high-speed quantum information encoding, while the reduction in domain wall density could minimize optical losses that currently limit the device performance. Given that BTO's electro-optic coefficient is ~30 times greater than conventional materials such as lithium niobate, the ability to optimize its domain configuration could enable modulators operating at GHz frequencies needed for quantum information processing applications. Combined with the technique's CMOS compatibility and room temperature processing, this approach provides a promising pathway toward realizing monolithic quantum photonic devices that integrate efficient modulation with other critical functionalities, such as photon generation and detection.

METHODS SUMMARY

Heterostructure growth

The BTO/LSMO heterostructure was grown by pulsed laser deposition from stoichiometric targets on a commercial DSO substrate at a deposition temperature of 700 °C. The laser fluence for BTO and LSMO was 1.0 and 2.0 kJ/cm², respectively. The layers were grown in an oxygen pressure of 0.05 and 0.2 mbar, respectively, followed by annealing for 5 min and a cooldown in 0.2 atm O₂.

He ion implantation

After film growth, Au films of 15 nm thickness have been deposited on top of the sample to serve as a buffer and neutralization layer for helium ion implantation. The sample was cut into smaller pieces, and various helium doses were implanted using a *SPECS IQE 11/35* ion source at an energy of 5 keV. Helium was chosen, since it is noble and a light element. It will, therefore, avoid charge doping and reduce defect creation. The ion distribution was simulated with the *SRIM 2013* software package. After implantation, the Au layers were mechanically removed.

X-ray diffraction

X-ray diffraction was carried out using a *Panalytical X'Pert* thin film diffractometer with Cu K_α radiation.

Second harmonic generation

A laser with 1000 nm wavelength, 150 fs pulse duration, and 1 MHz repetition rate was used. The light incident angle is kept constant at 45° with respect to the surface normal. The experimental setup and the fitting equations are described in more detail in the [supplementary material](#).

Phase field modeling

The evolution of the polarization was calculated by solving the time dependent Ginzburg–Landau equations. The framework and all Landau–Devonshire potential parameters were identical to the ones used by Li and Chen.¹² A model size of $64\Delta x \times 64\Delta x \times 48\Delta x$ was employed, with a grid spacing of $\Delta x = 1$ nm. The film and substrate thickness are $30\Delta x$ and $12\Delta x$, respectively.

Dielectric and ferroelectric properties

Circular capacitors with a radius of 25 μm were produced by depositing Au electrodes on the heterostructures using magnetron sputtering. Dielectric characterization has been performed using a *HP 4278A* LCR meter.

SUPPLEMENTARY MATERIAL

See the [supplementary material](#) for more details on the He implantation process, SHG analysis, and ferroelectric polarization measurements.

ACKNOWLEDGMENTS

This material was based on work supported by the U.S. DOE, Office of Science, Basic Energy Sciences, Materials Science and Engineering Division at Oak Ridge National Laboratory (synthesis and characterization). A.H. was funded by the German Research Foundation (DFG), Grant No. HE8737/1-1. The SHG spectroscopy measurement was supported by the U.S. Department of Energy, Office of Basic Energy Science, Division of Materials Sciences and Engineering (Ames National Laboratory is operated for the U.S. Department of Energy by Iowa State University under Contract No. DE-AC02-07CH11358). Synthesis and irradiation work was conducted as part of a user project at the Center for Nanophase Materials Sciences (CNMS), which is a U.S. Department of Energy, Office of Science User Facility at Oak Ridge National Laboratory.

AUTHOR DECLARATIONS

Conflict of Interest

The authors have no conflicts to disclose.

Author Contributions

Andreas Herklotz: Conceptualization (equal); Data curation (equal); Formal analysis (equal); Funding acquisition (equal); Investigation (equal); Methodology (equal); Software (equal); Supervision (equal); Validation (equal); Visualization (equal); Writing – original draft (equal); Writing – review & editing (equal). **Robert Roth:** Data curation (equal); Investigation (equal). **Zhi Xiang Chong:** Data curation (equal); Investigation (equal). **Liang Luo:** Data curation (equal); Formal analysis (equal); Investigation (equal). **Joong Mok Park:** Data curation (equal); Formal analysis (equal); Investigation (equal). **Matthew Brahlek:** Data curation (equal); Formal analysis (equal); Investigation (equal). **Jigang Wang:** Data curation (equal); Formal analysis (equal); Investigation (equal). **Kathrin Dörr:** Resources (equal). **Thomas Zac Ward:** Resources (equal); Supervision (equal); Writing – review & editing (equal).

DATA AVAILABILITY

The data that support the findings of this study are available from the corresponding author upon reasonable request.

REFERENCES

- ¹E. Gradauskaite, K. A. Hunnestad, Q. N. Meier, D. Meier, and M. Trassin, “Ferroelectric domain engineering using structural defect ordering,” *Chem. Mater.* **34**, 6468 (2022).
- ²G. Catalan, J. Seidel, R. Ramesh, and J. F. Scott, “Domain wall nanoelectronics,” *Rev. Mod. Phys.* **84**, 119 (2012).
- ³G. Sánchez-Santolino *et al.*, “A 2D ferroelectric vortex pattern in twisted BaTiO₃ freestanding layers,” *Nature* **626**, 529 (2024).
- ⁴H. F. Kay and P. Vousden, “XCV. Symmetry changes in barium titanate at low temperatures and their relation to its ferroelectric properties,” *London, Edinburgh Dublin Philos. Mag. J. Sci.* **40**, 1019 (1949).
- ⁵S. Abel *et al.*, “Large Pockels effect in micro- and nanostructured barium titanate integrated on silicon,” *Nat. Mater.* **18**, 42 (2019).

- ⁶W. Bogaerts, D. Pérez, J. Capmany, D. A. B. Miller, J. Poon, D. Englund, F. Morichetti, and A. Melloni, “Programmable photonic circuits,” *Nature* **586**, 207 (2020).
- ⁷F. Eltes *et al.*, “An integrated optical modulator operating at cryogenic temperatures,” *Nat. Mater.* **19**, 1164 (2020).
- ⁸H. Yu *et al.*, “Tuning the electro-optic properties of BaTiO₃ epitaxial thin films via buffer layer-controlled polarization rotation paths,” *Adv. Funct. Mater.* **34**, 2315579 (2024).
- ⁹K. J. Choi *et al.*, “Enhancement of ferroelectricity in strained BaTiO₃ thin films,” *Science* **306**, 1005 (2004).
- ¹⁰A. S. Everhardt, S. Matzen, N. Domingo, G. Catalan, and B. Noheda, “Ferroelectric domain structures in low-strain BaTiO₃,” *Adv. Electron. Mater.* **2**, 1500214 (2016).
- ¹¹A. R. Damodaran, E. Breckenfeld, Z. Chen, S. Lee, and L. W. Martin, “Enhancement of ferroelectric Curie temperature in BaTiO₃ films via strain-induced defect dipole alignment,” *Adv. Mater.* **26**, 6341 (2014).
- ¹²Y. L. Li and L. Q. Chen, “Temperature-strain phase diagram for BaTiO₃ thin films,” *Appl. Phys. Lett.* **88**, 072905 (2006).
- ¹³V. G. Koukhar, N. A. Pertsev, and R. Waser, “Thermodynamic theory of epitaxial ferroelectric thin films with dense domain structures,” *Phys. Rev. B* **64**, 214103 (2001).
- ¹⁴H. Guo *et al.*, “Strain doping: Reversible single-axis control of a complex oxide lattice via helium implantation,” *Phys. Rev. Lett.* **114**, 256801 (2015).
- ¹⁵A. Herklotz, A. T. Wong, T. Meyer, M. D. Biegalski, H. N. Lee, and T. Z. Ward, “Controlling octahedral rotations in a perovskite via strain doping,” *Sci. Rep.* **6**, 26491 (2016).
- ¹⁶M. Brahlek *et al.*, “Emergent magnetism with continuous control in the ultrahigh-conductivity layered oxide PdCoO₂,” *Nano Lett.* **23**, 7279 (2023).
- ¹⁷A. R. Mazza *et al.*, “Designing magnetism in high entropy oxides,” *Adv. Sci.* **9**, 2200391 (2022).
- ¹⁸A. Herklotz, S. F. Rus, C. Sohn, S. Kc, V. R. Cooper, E.-J. Guo, and T. Z. Ward, “Optical response of BiFeO₃ films subjected to uniaxial strain,” *Phys. Rev. Mater.* **3**, 094410 (2019).
- ¹⁹A. Herklotz, S. F. Rus, and T. Z. Ward, “Continuously controlled optical band gap in oxide semiconductor thin films,” *Nano Lett.* **16**, 1782 (2016).
- ²⁰E. Skoropata, A. R. Mazza, A. Herklotz, J. M. Ok, G. Eres, M. Brahlek, T. R. Charlton, H. N. Lee, and T. Z. Ward, “Post-synthesis control of Berry phase driven magnetotransport in SrRuO₃ films,” *Phys. Rev. B* **103**, 085121 (2021).
- ²¹M. Schmidbauer, A. Kwasniewski, and J. Schwarzkopf, “High-precision absolute lattice parameter determination of SrTiO₃, DyScO₃ and NdGaO₃ single crystals,” *Acta Crystallogr., Sect. B: Struct. Sci., Cryst. Eng. Mater.* **68**, 8 (2012).
- ²²M. C. Martin, G. Shirane, Y. Endoh, K. Hirota, Y. Moritomo, and Y. Tokura, “Magnetism and structural distortion in the La_{0.7}Sr_{0.3}MnO₃ metallic ferromagnet,” *Phys. Rev. B* **53**, 14285 (1996).
- ²³BaTiO₃ crystal structure, lattice parameters,” in *Ternary Compounds, Organic Semiconductors*, edited by O. Madelung, U. Rössler, and M. Schulz (Springer, Berlin, Heidelberg, 2000), pp. 1–6.
- ²⁴Y. Jiang *et al.*, “Enabling ultra-low-voltage switching in BaTiO₃,” *Nat. Mater.* **21**, 779 (2022).
- ²⁵S. A. Denev, T. T. A. Lummen, E. Barnes, A. Kumar, and V. Gopalan, “Probing ferroelectrics using optical second harmonic generation,” *J. Am. Ceram. Soc.* **94**, 2699 (2011).
- ²⁶J. Wang, K. Jin, H. Guo, J. Gu, Q. Wan, X. He, X. Li, X. Xu, and G. Yang, “Evolution of structural distortion in BiFeO₃ thin films probed by second-harmonic generation,” *Sci. Rep.* **6**, 38268 (2016).
- ²⁷D. J. Ascienzo, “Nonlinear optical studies of defects and domain structures in perovskite-type dielectric ceramics,” in Ph.D. thesis (CUNY Academic Works, 2017).
- ²⁸Z. Liu *et al.*, “Coherent transfer of lattice entropy via extreme nonlinear phononics in metal halide perovskites,” *PRX Energy* **3**, 023009 (2024).
- ²⁹Z. Liu *et al.*, “Coherent band-edge oscillations and dynamic longitudinal-optical phonon mode splitting as evidence for polarons in perovskites,” *Phys. Rev. B* **101**, 115125 (2020).
- ³⁰R. Guo *et al.*, “Tailoring self-polarization of BaTiO₃ thin films by interface engineering and flexoelectric effect,” *Adv. Mater. Interfaces* **3**, 1600737 (2016).

³¹H. Lee *et al.*, “Imprint control of BaTiO₃ thin films via chemically induced surface polarization pinning,” *Nano Lett.* **16**, 2400 (2016).

³²S. Saremi, R. Xu, L. R. Dedon, J. A. Mundy, S.-L. Hsu, Z. Chen, A. R. Damodaran, S. P. Chapman, J. T. Evans, and L. W. Martin, “Enhanced electrical resistivity and properties via ion bombardment of ferroelectric thin films,” *Adv. Mater.* **28**, 10750 (2016).

³³S. Saremi, R. Xu, L. R. Dedon, R. Gao, A. Ghosh, A. Dasgupta, and L. W. Martin, “Electronic transport and ferroelectric switching in ion-bombarded, defect-engineered BiFeO₃ thin films,” *Adv. Mater. Interfaces* **5**, 1700991 (2018).

³⁴Y. L. Li, L. E. Cross, and L. Q. Chen, “A phenomenological thermodynamic potential for BaTiO₃ single crystals,” *J. Appl. Phys.* **98**, 064101 (2005).